UNIVERSITATEA NAȚIONALĂ DE ȘTIINȚĂ ȘI TEHNOLOGIE POLITEHNICĂ DIN BUCUREŞTI

FACULTATEA ŞTIINŢA ŞI INGINERIA MATERIALELOR

Autoare: Ing. Gabriela CIUNGU (PETRE)

TEZĂ DE DOCTORAT

Conducător de doctorat: Prof. habil. dr. ing. Brânduşa GHIBAN

Prof. dr. ing. Ilare BORDEAŞU

București 2024

STUDIES AND EXPERIMENTAL RESEARCH ON THE CAVITATION AND BIODEGRADATION BEHAVIOR OF SOME ZnCu(Mg) ALLOYS

CUPRINS

PART I-CURRENT STAGE OF THE DEVELOPMENT OF BIODEGRADABLE ZINC ALLOYS

CHAPTER 1. ZINC AS A POTENTIAL BIOBORBIBLE METAL

Metals have a long history of use as implant material in the medical field [1-7]. The appeal of using metals is attributed to their unique combination of properties, including good mechanical strength, ductility, toughness, wear resistance and formability. From the point of view of biocompatibility, the first generation of metallic materials used for implant applications had to be inert in the physiological environment.

1.1. Requirements of a biodegradable metal for stent and bone fixation device

Biodegradable metals are best suited for implants that require temporary functions in the body. Two promising medical applications of bioabsorbable metals are in the manufacture of stents and orthopedic fixation devices. A stent is a miniature tube that is placed in a hollow body structure such as a blood vessel or urethra [24]. The main function of the stent is to keep the luminal structure open and relieve constrictions. The stent can be delivered through various medical procedures, such as percutaneous coronary intervention (PCI) to treat cardiac artery stenosis [25].

In orthopedics, an internal fixator is an implant that is used to guide the healing process of bone fractures. The implant stabilizes the fractured bone, thus preventing movement along the fracture lines and allowing the damaged structures to heal quickly. Orthopedic internal fixators can be in the form of plates and screws, wires (eg, Kirschner wires), and nails (eg, intramedullary rod) [26].

1.2 Zinc as a metal for orthopedic biomedical applications

In the search for a bioabsorbable implantable material, current research has developed two unanimously accepted types of materials. The first type is the polymeric material, in vitro biocompatibility studies of polyglycolic acid/polylactic acid (PGA/PLA), polycaprolactone (PCL), polyhydroxybutyrate valerate (PHBV), polyorthoester (POE) and polyethylene oxide/polybutylene terephthalate (PEO/PBTP) being among the first to be reported [41-43]. These studies eventually led to the development of commercial bioabsorbable implants. Examples include the Igaki-Tamai, DESolve and ABSORB stents, made from polylactic acid (PLLA) [44].

Ideal BioStent consisting of salicylic acid/ adipic acid (SA/AA); and the REVA stent constructed from tyrosine-derived polycarbonate [14,31]. There are also reports of the successful application of polymer-based bioabsorbable screws for bone graft fixation [45].

The second class of bioabsorbable materials are metallic materials. **Table 1.1** summarizes the advantages and disadvantages of the most promising biodegradable metals, namely Mg, Fe and Zn. These metals are considered essential micronutrients of the body, with the table including the

Recommended Daily Intake (RDI) for each metal. It is suggested that IDR is a key measure for assessing the biocompatibility of a material [11].

Table 1.1-Advantages and disadvantages of biodegradable metals based on magnesium, iron and zinc [9,11,12,15,23,55,]

Biodegradable metal	Recommended daily dose, mg	Benefits	Disadvantage
Mg	375-700	Excellent biocompatibility Compact corrosion product Good resistance Low density and modulus of elasticity (close to bone properties) Compatible with MRI	Excessive corrosion rate Low strength and limited formability Evolution of hydrogen gas Premature loss of mechanical integrity Unwanted increase in pH Susceptible to stress corrosion cracking
Fe	10-20	Good biocompatibility Excellent strength and formability Compatible with IRM (austenitic phase) No gases are generated during degradation	Corrosion rate too slow Bulky corrosion product that accumulates and repels adjacent tissues
Zn	6,5-15	Good biocompatibility Corrosion rate between that of magnesium and iron No gases are generated during degradation Low melting point and low reactivity in the molten state	Corrosion rate too slow Bulky corrosion product that accumulates and repels adjacent tissues Weaker mechanical properties Aging hardening

Chapter 2. Development of zinc and zinc alloys for biomedical applications

Research on biodegradable Zn and zinc-based alloys for biomedical applications is relatively new, with most papers published within the last ten years. However, some of the first mentions of Zn being used as a potential biodegradable implant include those of Bolz and Pop [68], who suggested in a 2001 patent the feasibility of bioabsorbable coronary stents made of pure Zn and some Zn alloys -X (X= Ti, Ca); and by Wang et al. [69] in 2007. Fig. 2.1 shows a possible development of zinc and its alloys, depending on the alloying elements introduced.

Fig. 2.1 Design of Zn alloys for biodegradable applications [after 187]

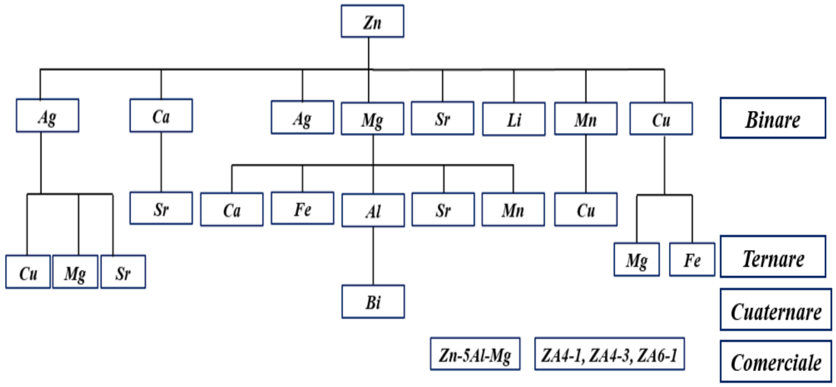

2.1 Pure zinc

In 2011, Vojtech et al.[19] published what appears to be the first study on biodegradable Zn (99.95%) and other Zn alloys and essentially began formal research into the use of this metal for bioabsorbable implant applications. They observed, following in vitro biodegradability tests, that Zn does indeed corrode in a physiological fluid. Also, although he did not perform any biocompatibility tests, he observed that the dose of Zn ions released by corrosion is negligible compared to the maximum tolerable biological limit. He then concluded that Zn is not likely to cause a toxic response if used as an implant and is therefore a possible alternative to biodegradable Mg-based alloys.

2.2. Binary alloys

The main purpose of adding alloying elements to Zn is to modify two properties: (i) mechanical properties and (ii) biocorrosion properties. The most logical approach to Zn alloying for biomedical applications is to combine it with elements known to be biocompatible or essential for human function, such as Mg, Ca, and Cu. Magnesium is the best known and most studied biodegradable metal. It is therefore not surprising that a substantial number of studies have looked at the combination of Mg and Zn. Vojtech et al. [19], in 2011, were the first to report the use of Zn-Mg alloy for bone fixation applications. Development of binary Zn alloys continued with notable work by Zheng et al [87,88] on Zn–Mg, as well as zinc–calcium (Zn–Ca) and zinc–strontium (Zn–Sr) alloys.

2.3. Ternary alloys

Vojtech et al. [19] were also the first to report the biocompatibility of a ternary Zn alloy, namely zinc-aluminum-copper (Zn-Al-Cu). Studies on other ternary combinations have been equally well studied, most of them based on the Zn-Mg combination. Some of the reported Zn-Mg ternary alloys include zinc-magnesium-iron (Zn-Mg-Fe) [114], zinc-magnesium-strontium (Zn-Mg-Sr) [88,115], zinc-magnesium-calcium (Zn-Mg-Ca) [88] and zinc-magnesium-manganese (Zn-Mg-Mn) [116].

2.4. Quaternary alloys Currently, there are few reports on the use of quaternary Zn alloys. Only one study may be cited; namely, the study by Bakhsheshi-Rad et al. [122], who analyzed the zinc-magnesium-aluminum-bismuth (Zn-Mg-Al-Bi) combination.

2.5. Commercial alloys

Some commercially available Zn alloys have also been studied as a possible biodegradable implant material. Commercial alloys offer the distinct advantage of good accessibility and predictable composition. Wang et al. [123] investigated the biodegradability and biocompatibility of ZA4-1 (3.5-4.5 Al, 0.75-1.25 Cu, 0.03- 0.08Mg), ZA4-3 (3.5-4.3Al , 2.5-3.2 Cu, 0.03-0.06Mg) and ZA6-1 (5.6-6.0 Al, 1.2-1.6 Cu) Zn alloys, while Kannan et al. [124] studied similar properties in Zn-5Al-4 Mg alloys.

Chapter 3. Mechanical properties of biodegradable zinc

Zinc is not famous for its good mechanical properties. Zinc has lower flow and tensile strength compared to Mg or Fe. As previously mentioned, one of the issues raised against zinc, particularly when used for cardiovascular stent applications, is its poor strength. Stent materials should have a tensile strength of about 300 MPa, while pure Zn has a tensile strength of about 28–120 MPa [21].Pure cast Zn is not technologically useful because it exhibits poor ductility (2–2.5%) at room temperature [135,136]. Zn adopts the hexagonal close-packed (HCP) structure, which inherently imparts poor ductility and toughness to the as-cast structure [137]. On the other hand, pure machined Zn exhibits excellent ductility with an elongation at break of 60–80% (tested parallel to the rolling direction) [136]. This high level of ductility in wrought Zn will be crucial in the fabrication of stents. Stents are usually small hollow tubes with typical diameters of approximately 2.5–3.0 mm [138] and strut thicknesses of 70–175 mm [138,139].

3.1. Influence of alloying elements Alloying refers to the process of adding impurities to improve the properties of a metal. Alloying alters the properties of the host metal by inducing a change in the microstructure and triggering a related hardening mechanism. For example, impurities that are dissolved in a single-phase microstructure cause solid solution hardening, while alloying elements that create a second-phase precipitate cause precipitation hardening [137]. For biodegradable Zn, the mechanical properties of the alloy can be influenced by (i) the type, 15 (ii) the number, and (ii) the amount or concentration of alloying elements, as noted in Table 1.1.

Fig. 3.1 shows an Ashby diagram comparing the reported mechanical properties (i.e., ductility or elongation at break, ef vs. tensile strength, UTS) of various Zn compositions, including (i) pure alloys, (ii) binary, (iii) ternary, and (iv) quaternization. The lines represent the target UTS (300 MPa) and ef (18 %) suitable for some biomedical applications. This graph can help us understand the influence of alloying elements on the properties of Zn.

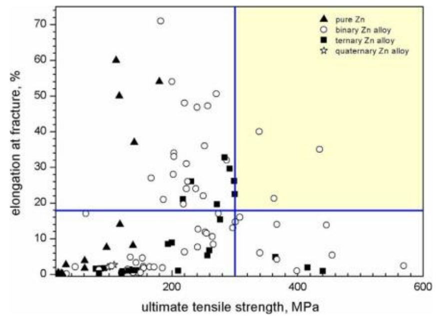

Fig. 3.1. Graph of elongation at break (%) vs yield strength according to the number of Zn alloying elements. The superimposed lines represent the standard ratings required for materials used for cardiovascular and orthopedic medical applications. The colored region represents the space of acceptable properties [187]

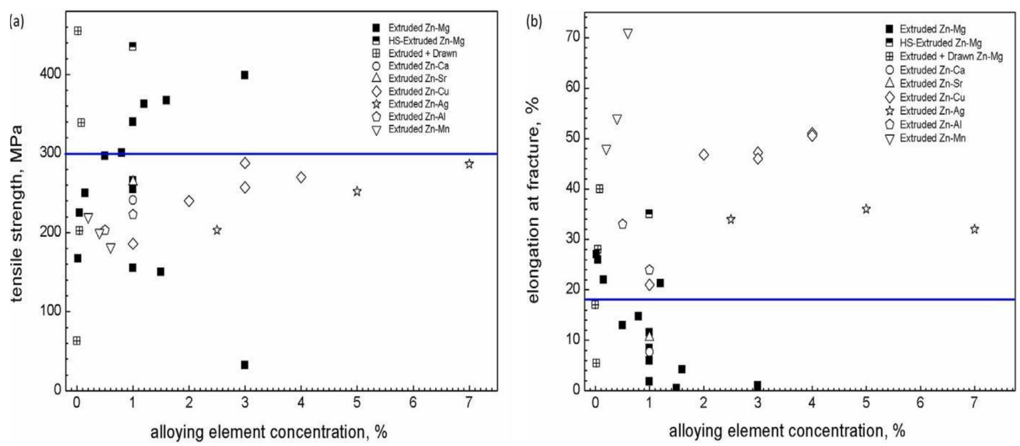

Fig. 3.2. Plot of (a) tensile strength and (b) elongation at break (%) as a function of alloying element concentration (%) for various binary Zn alloys formed by extrusion [187]

Fig. 3.2 (a) and (b) show the fracture toughness and ductility as a function of alloying element proportion (%) for various binary Zn alloys (i.e. Mg, Ca, Sr, Cu, Ag, Al and Mn), respectively. This comparison is made between alloys formed by a single type of manufacturing technique (ie extrusion, including the hot isostatic extrusion variant) only to remove the influence of the manufacturing method. For example, at a composition of 1%, the strength and ductility of the Zn alloy varied with the alloying element (eg, Mg, Sr, Ca, Al, Cu).

Chapter 4. Biodegradation and biocompatibility of zinc

4.3. In vitro biodegradability of Zn alloys

In some of the studies that used polarization tests, the corrosion rate was reported in terms of corrosion current density. While comparing in vitro biocorrosion rate results with in vivo results is certainly inadvisable, comparing in vitro degradation rates reported by different studies and obtained under different experimental conditions is equally questionable.
Indeed, it is rare to find even agreement between corrosion rates obtained from polarization and immersion tests performed in a single study. A quick scan of Table 2 shows that the reported in vitro tests, primarily the polarization and immersion tests, were performed under different test

conditions, such as different physiological solutions and immersion times. These test parameters, along with others such as scan speed, electrolyte gas exchange, ratio of specimen surface area to electrolyte volume, pH buffering techniques, and flow conditions, can influence the corrosion behavior of the test specimen. [151,167].

4.4. In vitro biocompatibility of Zn alloys

Cytotoxicity tests, which assess the ability of a substance to destroy living cells, and hemocompatibility tests, which assess the interaction between a substance and blood, are the most commonly used tests to assess the biocompatibility of Zn. Antibacterial tests are mainly popular for cases where Zn is alloyed with known antibacterial elements such as Cu and Ag. Other tests to determine genotoxicity, mutagenicity, cellular functionality and inflammatory response were also performed on biodegradable Zn.

PART II OWN EXPERIMENTAL RESEARCH

CHAPTER 5 Materials, methodology and experimental program

5.1 Materials and methodology

To make the experimental materials, the experimental zinc alloys were developed in a classic furnace, cast and prepared for structural investigations. Because casting allows easy adjustment of the alloy composition, mass production of Zn-based alloys is achieved through this process. The casting alloy processing process involves melting parts of the alloy, pouring the molten metal into a mold, and finally solidifying. Melting took place in an induction furnace at a typical temperature of 450–650 °C.

Aliaj	Chemical composition, %gr							
	Mg	Cu	S	P	Si	Fe	Ni	Zn
Zn	-	-	0.36	0.019	0.45	-	0.009	Rest
ZnCuAl	0.35	2.36	0.15	0.146	0.97	0.39	0.019	Rest
ZnCuMg	3.66	3.05	0.14	0.001	0.36	0.95	0.02	Rest

Table 5.1- Chemical composition of experimental zinc alloys

In **fig. 5.1** the experimental program drawn up in such a way as to lead to the fulfillment of the initially proposed major objectives is shown.

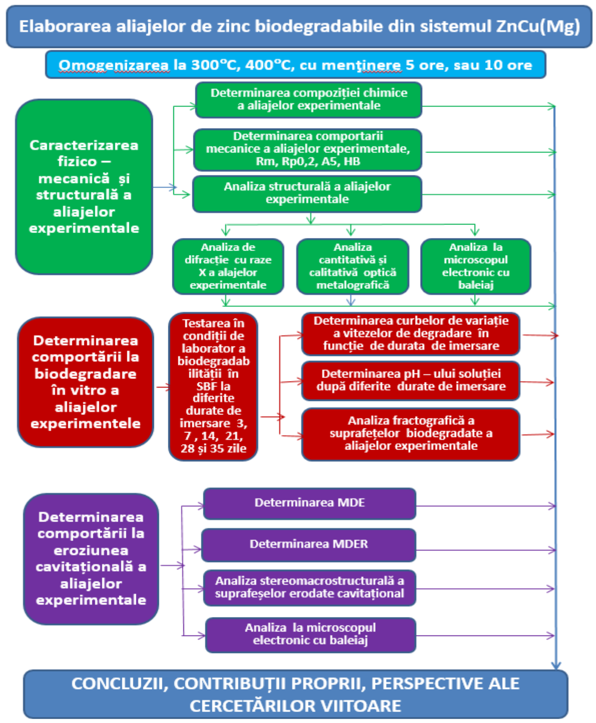

Fig. 5.1- Experimental program

CHAPTER 6 PHYSICAL-MECHANICAL CHARACTERIZATION OF EXPERIMENTAL ZINC ALLOYS

6.1 Mechanical behavior of zinc alloys in the ZnCu(Mg) system

Alloy	State	Resistance to breaking, R_m, (MPa)	Drip limmit, R_p, (MPa)	Elongation to break, A_5(%)	Modulus of elasticity, E, (MPa)
ZnCu	martor	80	67.87	4.06	4.95
	300^0C/5h	94	49.08	4.14	11.03
	300^0C/10h	98	29.54	4.22	22.27
	400^0C/5h	90	31.96	3.35	15.17
	400^0C/10h	75	33.19	2.04	20.03
ZnCuMg	martor	123	84.23	2.42	13.12
	300^0C/5h	180	84.93	3.24	14.55
	300^0C/10h	200	56.96	6.75	15.82
	350^0C/5h	162	57.64	3.87	13.78
	350^0C/10h	138	52.56	3.34	14.87

Table 6.1- The mechanical characteristics of the investigated zinc alloys, from the ZnCu(Mg) system

Table 6.1 shows the values of the mechanical characteristics resulting from their processing, of zinc and experimental zinc alloys. From the analysis of the stress-strain curves in fig. 6.1 highlights the fact that the homogenization treatment applied to pure zinc at 400°C/5h is the one that gives it the best tenacity, since the area under the curve is the largest, compared to the other results. Similar results regarding the toughness of the experimental alloys can be observed for the other experimental alloys. Thus, the same homogenization treatment at 400°C/5h is observed either in the ZnCu alloy (fig. 6.2) or in the ZnCuMg alloy (fig. 6.3), which gives them maximum toughness.

For a complete analysis regarding the mechanical behavior, histograms of each mechanical characteristic obtained, depending on the structural state, were made in fig. 6.4 (for zinc), fig. 6.5 (for ZnCu alloy) and fig. 6.6 (for ZnCuMg alloy).

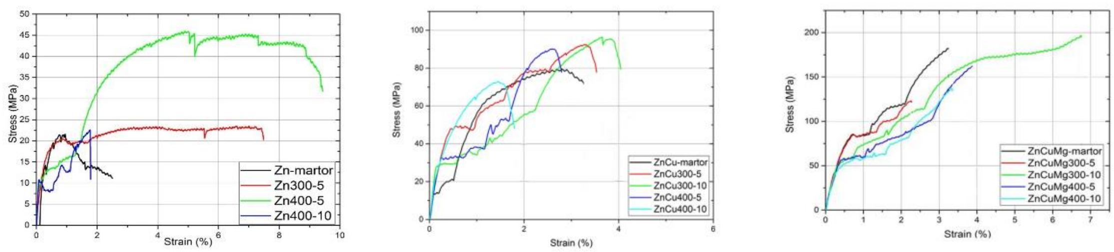

Fig. 6.1-6.3.The appearance of the tensile curves of Zn(6.1), ZnCu(6.2), ZnCuMg(6.3)

Analysis of the results presented in fig. 6.4 highlights the evolution of the mechanical characteristics of the experimental ZnCu alloy according to the homogenization thermal treatment applied. It is noted that at a 300°C/10h homogenization, the highest mechanical strength is obtained, respectively 100MPa (fig. 6.5a), the highest yield strength, respectively 68MPa (fig. 6.5b) and the highest elongation , respectively 4.13% (fig. 6.4c). On the other hand, homogenization at 300°C/10h leads to obtaining the highest modulus of elasticity, respectively 22.27 MPa (fig. 6.4d).

Analysis of the results presented in fig. 6.5 highlights the evolution of the mechanical characteristics of the experimental ZnCuMg alloy according to the homogenization thermal treatment applied. It is noted that at a homogenization of 300°C/10h, the highest mechanical strength is obtained, respectively 200MPa (fig. 6.5a), the highest elongation, respectively 6.8% (fig. 6.5c) and the highest modulus of elasticity, respectively 15.82MPa. Instead, homogenization at 300°C/5h leads to obtaining the highest yield strength, respectively 84.93 MPa (fig. 6.5b).

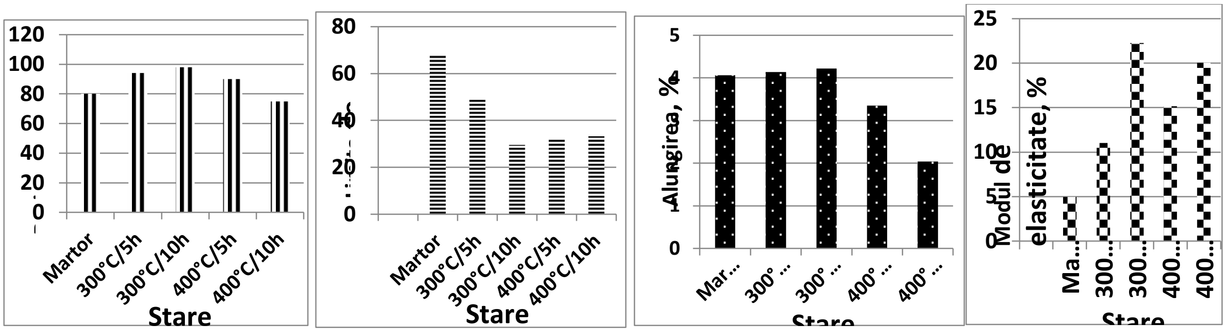

Fig.6.4 – Histograms of the mechanical characteristics of the ZnCu alloy, in different structural states: a-mechanical resistance; b- yield strength; c- elongation; d- modulus of elasticity

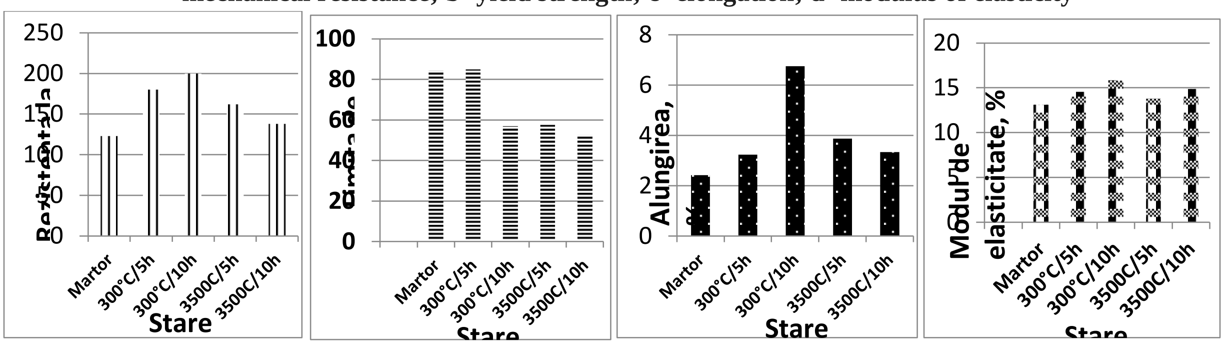

Fig.6.6 The variation of the mechanical characteristics of the ZnCuMg alloy, in different structural states: a-mechanical resistance; b- flow limit; c- elongation; d- modulus of elasticity

6.2 Stereomacrostructural fractographic analysis of tensile specimens

Macrofractographic analysis of the tensile specimens, performed under a stereomicroscope, both in longitudinal and cross-section, allowed the evaluation of the fracture surfaces after testing the mechanical characteristics, as well as the critical analysis of the fracture mode of the experimental zinc alloys compared to zinc pure in different structural states. In the case of the ZnCu system, the surfaces are typical of fragile, transgranular, transcrystalline breaks, with a bright crystalline appearance, with very fine annealing loops and areas with numerous intermetallic compounds. The fractographic aspects are similar, both in the control sample (fig. 6.12), with crushed grains and bright crystalline appearance, and in the homogenized samples, where no significant fractographic changes are recorded. Note the blue coloring of the various crystallized zones in the fracture surfaces of this alloy.

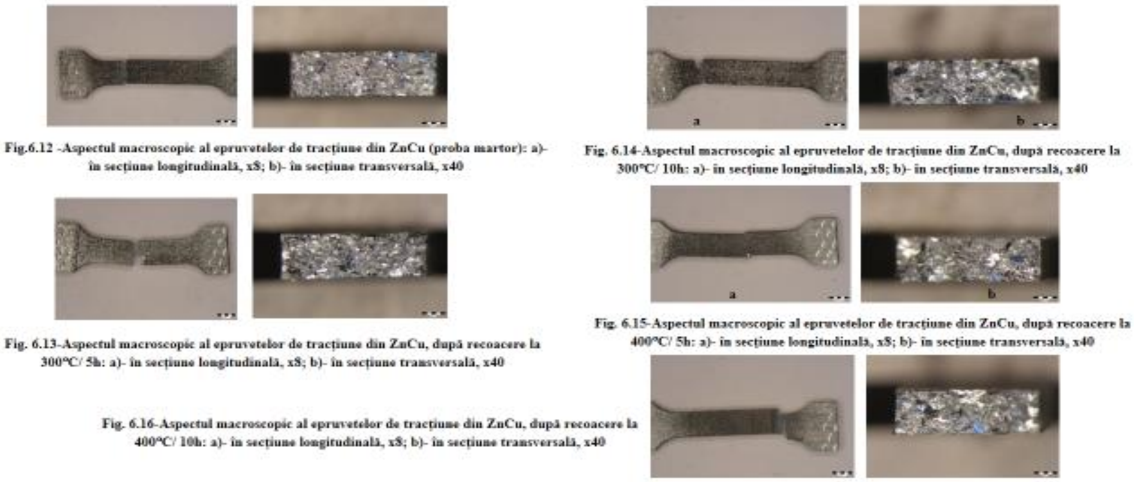

Fig. 6.12-6.16.The macrostructural aspects of the tensile fracture surfaces of the ZnCu alloy specimens

If in the control sample the appearance is specific to a sudden brittle break, with fine grain, with solidification loops and with large differences in relief, in the homogenized samples a finish of the grain and fine transcrystalline breaks, with a shiny appearance, can be noted. The surfaces are mixed, with areas with crushed grains and fine areas with the abundant presence of intercrystalline compounds (fig. 6.19). No significant differences are observed between the surfaces with different thermal homogenization treatments. Noteworthy is the blue color of the various matted areas, generated by the complex alloying and the differentiated crystallographic orientation of the grains.

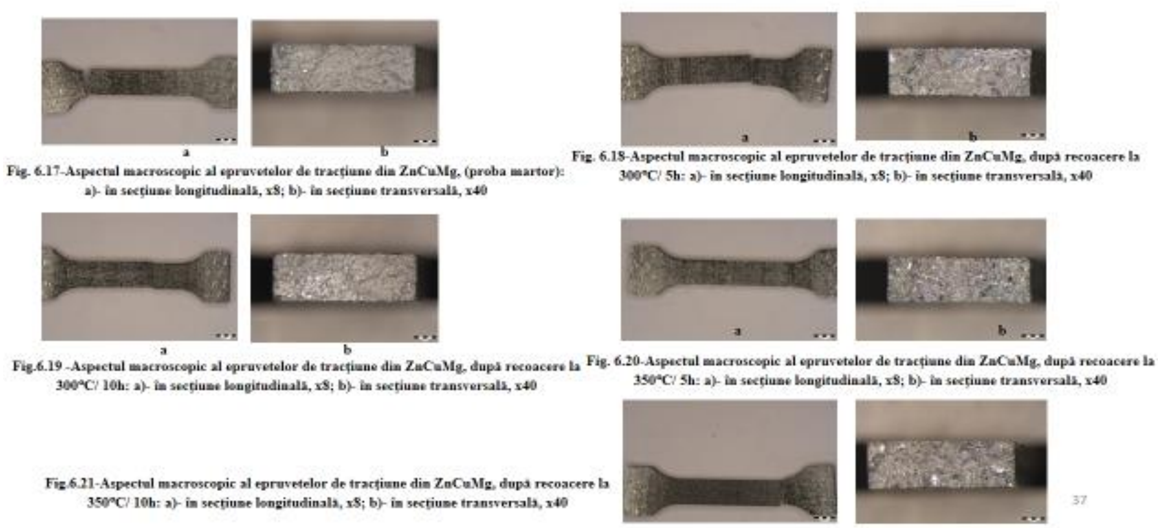

Fig.6.17-6.21.The macrostructural aspects of the tensile fracture surfaces of the ZnCuMg alloy specimens

Chapter 7. Structural characterization of experimental Zn alloys

Fig. 7.22- Aspecte structurale ale aliajului ZnCu, stare turnat (proba martor): a- x500; b- detaliu al imaginii a (x1000)

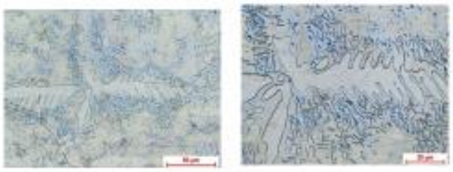

Fig.7.23 Aspecte structurale ale aliajului ZnCu, stare turnat şi omogenizat la 300°C/5ore: a- x500; b- detaliu al imaginii a (x1000)

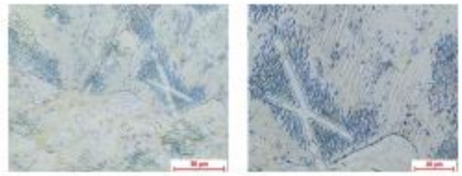

Fig. 7.24- Aspecte structurale ale aliajului ZnCu, stare turnat şi omogenizat la 300°C/10 ore: a- x500; b- detaliu al imaginii a (x1000)

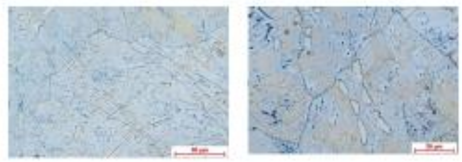

Fig.7.25 - Aspecte structurale ale aliajului ZnCu, stare turnat şi omogenizat la 400°C/5 ore: a- x500; b- detaliu al imaginii a (x1000)

Fig. 7.22-7.25.Structural aspects of the ZnCu alloy, control sample and after homogenization

The results of the structural analysis performed with the optical metallographic microscope allowed the identification of the phases and structural constituents of the biodegradable zinc alloys. In fig. 7.22 of the slide shows a structure made up of primary compounds of Cu5Zn6 in the shape of the letter epsilon and a lamellar interdendritic eutectic, consisting of solid solution based on zinc and intermetallic compounds. In fig. 7.23, the primary dendritic structure of the casting homogenizes, after a 5-hour hold, not completely removing. Longitudinal axis dendrites with intergranular separation are still noticeable. In fig. 7.24 the dendrite becomes island, the compound and lamellar eutectic. At 400 degrees they completely disappeared and the compounds remained. Increasing the homogenization temperature to 400 C (either 5 hours or 10 hours), in fig. 7.25 determines the complete elimination of the inhomogeneous dendritic casting structure and the highlighting of the granular structure, in which Cu5Zn6 compounds have polyhedral, island forms, with intragranular precipitation.

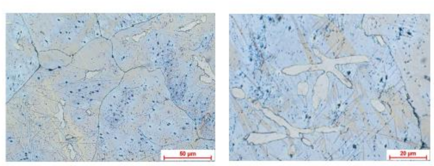

Fig. 7.26- Aspecte structurale ale aliajului ZnCu, stare turnat şi omogenizat la 400°C/10 ore: a- x500; b- detaliu al imaginii a (x1000)

Fig. 7.26- Structural aspects of the ZnCu alloy, as cast and homogenized at 400°C/10 hours: a- x500; b- detail of image a (x1000)

At 400 degrees/10 h, as can be seen from fig. 7.26, the dendrites completely disappeared and the compounds remained.

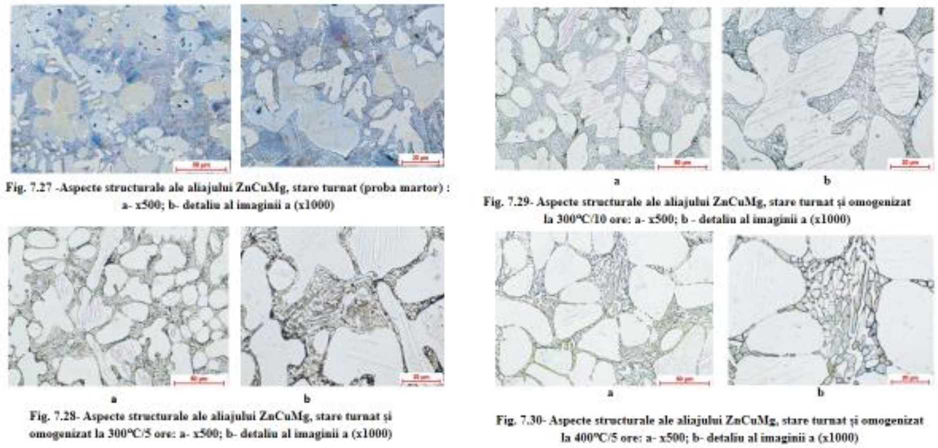

Fig. 7.27-7.30.Metallographic analysis of Zn alloys from the ZnCuMg system

The structural aspect of the ZnCuMg complex alloy in the cast state is shown in fig. 7.27.- eutectic, dendritic solid solution and compounds. During homogenization, two phenomena started: 1. the dendrite becomes island and 2. the globular lamellar eutectic. Islands have macles. The application of thermal homogenization treatments causes the globulization of the eutectic and the elimination of dendrites in island forms.

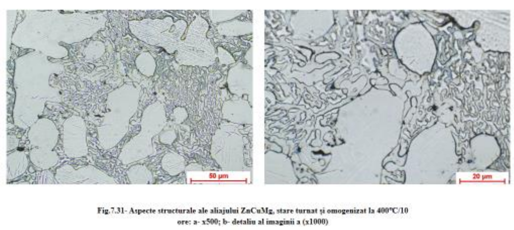

Fig.7.31. Metallographic analysis of Zn alloys from the ZnCuMg system

In the ternary alloy, the structure changes, as can be seen from fig. 7.31, the eutectic becomes lacy, we still have solid soil of Mg and Cu in Zn.

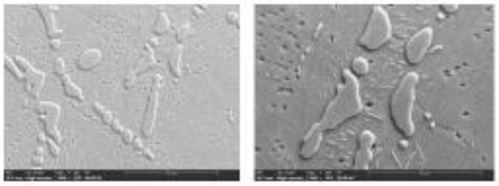

a b

Fig. 7.32- Imagini SEM ale aliajului ZnCu, stare turnat (proba martor):
a- x1000; b- detaliu al imaginii a (x2000)

Zona	Micro-compoziție locală, %gr.	
	Cu	Zn
1	1,98	95,85
2	3,64	96,36
3	12,54	87,29
4	1,86	98,14

f

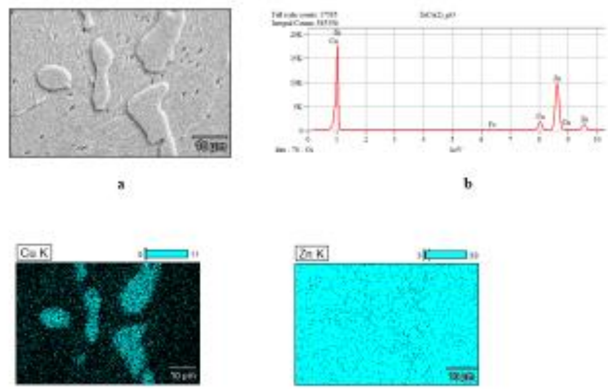

a b c d

Fig. 7.33- Analiza la microscopul electronic cu baleiaj a aliajului binar ZnCu:
a. imagine SEM; b- EDAX; c distribuția cuprului;
e- distribuția zincului; f- microcompoziție locală

Fig. 7.32-7.33. Scanning electron microscope analysis of alloys from the ZnCuMg system

In fig. 7.32 shows the appearance under the scanning electron microscope which indicates a structure with large grains in which intermetallic compounds based on ZnCu are present. In fig. 7.33- we have the distribution of secondary electrons indicating Cu or Zn. Also, the local chemical microcomposition that demonstrates the presence of Cu and Zn in the binary alloy and the rendering of the weight of each element in the table.

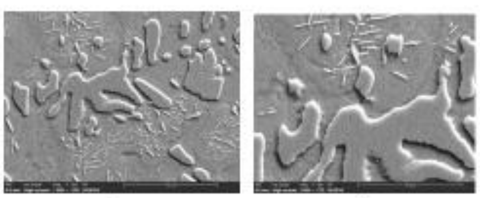

a b

Fig. 7.34- Imagini SEM ale aliajului ZnCuMg, stare turnat (proba martor):
a- x1000; b- detaliu al imaginii a (x2000)

Zona	Micro-compoziție locală, %gr.		
	Mg	Cu	Zn
1	0	3,99	96,01
2	1,96	3,22	94,52
3	0	2,25	97,75
4	0	11,17	88,83

f

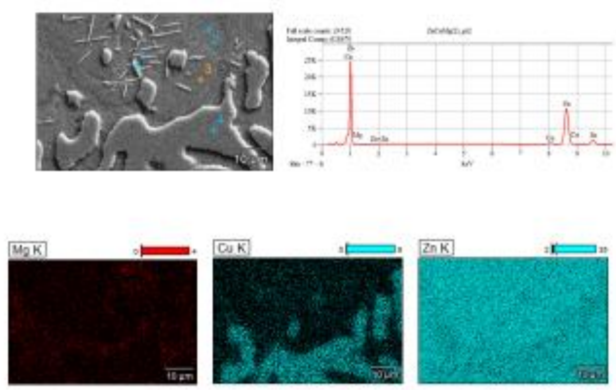

c d e

Fig. 7.35- Analiza la microscopul electronic cu baleiaj a aliajului complex ZnCuMg:
a. imagine SEM; b- EDAX; c- distribuția magneziului; d- distribuția cuprului;
e- distribuția zincului; f- microcompoziție locală

Fig. 7.34-7.35. Scanning electron microscope analysis of alloys from the ZnCuMg system

The complex alloying of Zn with Cu and Mg creates a zinc-based solid solution structure, in which intermetallic compounds with different shapes and distributions are present, as well as the presence of a lamellar herringbone-shaped eutectic (fig. 7.34). and next to insular intermetallic compounds in the metal matrix made of zinc-based solid solution. In fig. 7.35 - the distribution of Mg, Cu and Zn and also the local microcompositions with the weight of each element in the bottom left (f).

Chapter 8. Biodegradation behavior of Zn-based alloys from the ZnCuMg system. Corrosion and biodegradation mechanisms

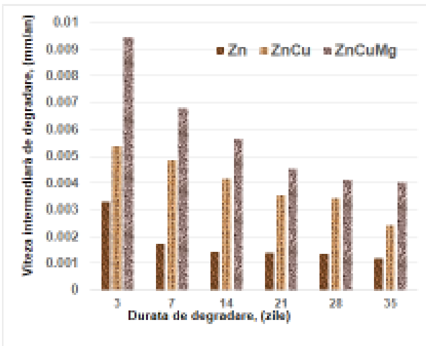

Fig 8.2 Variaţia vitezelor intermediare de degradare în funcţie de durata de degradare a aliajelor biodegradabile experimentale de zinc din sistemul ZnCu(Mg)

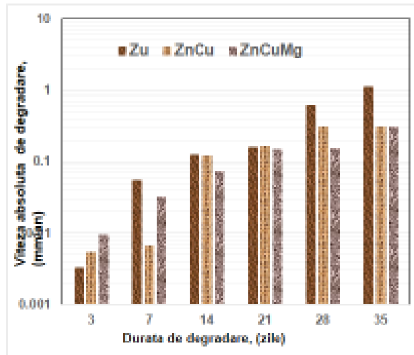

Fig 8.3 Variaţia vitezelor absolute de degradare funcţie de durata de degradare a aliajelor biodegradabile experimentale de zinc din sistemul ZnCu(Mg)

Fig. 8.2-8.3.The variation of the intermediate and absolute degradation rates depending on the degradation time of the experimental biodegradable Zn alloys from the ZnCuMg system

The results regarding the biodegradation behavior of zinc alloys, compared to pure Zn, in a human fluid simulation solution, can be seen in fig 8.2 of the image that Zn has a fairly good biodegradation behavior, registering monotonically decreasing losses with small values. notices a certain plateau in the degradation rates starting from the 14th day of immersion, with very low speeds, below 0.0015mm/year. The presence of copper in the zinc alloy causes a considerable increase in the rates of intermediate biodegradation, so that this rate then progressively decreases to approximately 50% of the 3-day value. The pattern of variation in the ZnCu binary alloy is similar to the variation of zinc intermediate velocities. It can be naturally concluded that the simultaneous alloying of Cu and Mg in Zn causes a more weighted biodegradability behavior than that of Zn, which means a better stability of the future biodegradable implant.

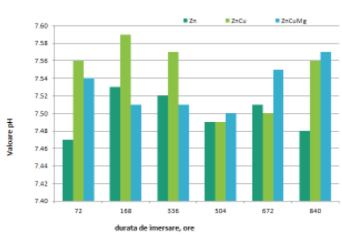

Fig. 8.4 Evoluţia valorilor de pH pe durata de imersare a probelor în SBF

- ✓ Zn- cele mai mici valori ale pH-ului, cuprins intre 7,47 şi 7,53;
- ✓ ZnCu- cele mai mari valori ale pH-ului , aflate in intervalul 7,49- 7,59;
- ✓ ZnCuMg- se obţin valori intermediare ale PH-ului, respectiv 7,49 ÷ 7,59

Fig.8.4.Analysis of the PH variation of the SBF simulant solution

It is noted that after immersion periods of 3, 7 and 14 days, the highest ph values are obtained, respectively 7.56 ÷ 7.59, the lowest value being obtained after 21 days of removal.

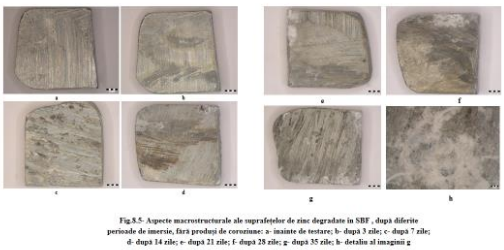

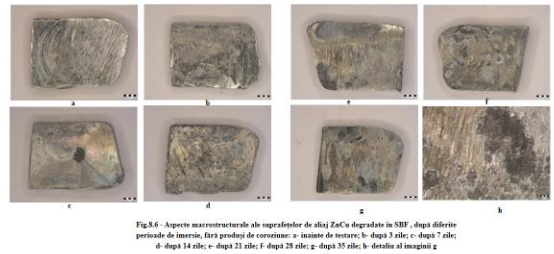

Fig.8.5-8.6. Microstructural aspects of Zn, Zn Cu surfaces degraded in SBF after different periods of immersion

The macrostructural aspects of the degraded surfaces at different immersion times in SBF, and after the removal of the corrosion products of the experimental alloys are shown in fig. Above. Degradation of Zn starts slowly, even after the first removal, from 3 days. The biodegradation process is slow, proceeding with material pulling and dissolving in small quantities, so that after 35 days the appearance of corrosion points can be noticed on the test surfaces, initiated, as a rule, on material discontinuities. The entire surface is covered with corrosion points, but only sporadically, a sign of a relatively slow biodegradation, fig. 8.5h.

In the binary ZnCu alloy, the same slow biodegradation process is noted, with the deepening of the degradation zones slowly and continuously, until the last removal time of 35 days. Also, the biodegradation is initial on the discontinuity zones of the exposed surfaces and becomes more and more aggressive until the last immersion time. The appearance of the degraded areas after 35 days, highlighted in fig. 8.6h, shows the development of areas with localized degradation, with great depths of up to 0.05mm.

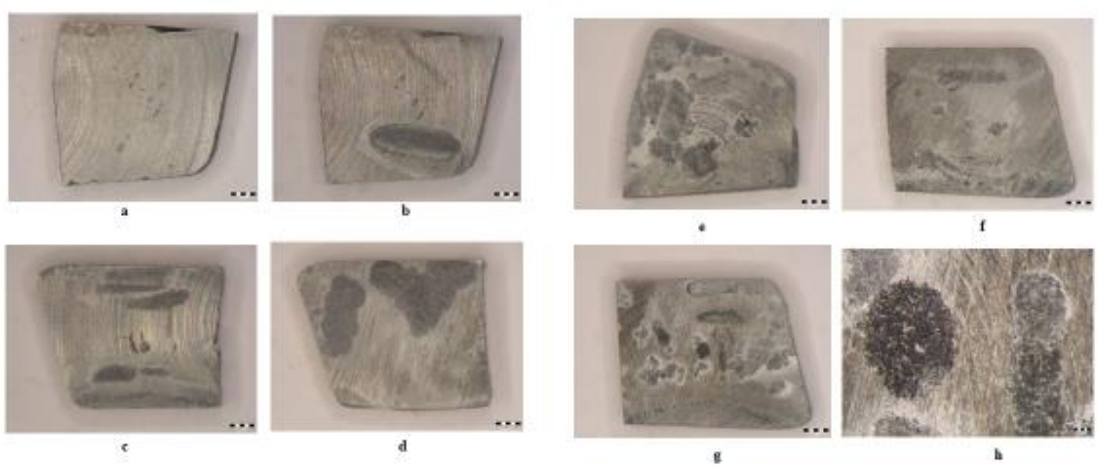

Fig.8.7. Microstructural aspects of ZnCuMg surfaces degraded in SBF after different periods of immersion

The complex alloy ZnCuMg has a behavior similar to that of Zn. Biodegradation starts very slowly, even from the first removal, of 3 days, and continues progressively slowly, until the last removal of 35 days. It is also noticeable an interconnected network of corrosion points, with relatively small depths, in fig. 8.6 h. It is also noted that the degradation process is less obvious than in the binary alloy, ZnCu. The comparison of the experimental results from this paper with the data from the specialized literature confirms that alloying changes the biodegradation behavior of Zn-based alloys, on the one hand, and the values obtained are comparative and even unexpected for a complex alloy chosen in the paper. Thus, regardless of the alloying method, in similar human environments, the degradation of either Zn or the various zinc-based alloys takes place.

CHAPTER 9 CAVITATION EROSION BEHAVIOR OF EXPERIMENTAL ZINC ALLOYS IN THE ZnCu(Mg) SYSTEM

The results of the cavitation test are expressed by diagrams containing the experimental values of the three samples (red, green, black and blue color points), tested from each state of heat treatment and the specific averaging curves, which give the variation of the cumulative average depth of erosion MDE(t) and its speed MDER(t). They are the basis of the characterization of the behavior and resistance of the surface structure to the erosive stresses of the vibrating cavitation microjets. The diagrams, built on the basis of the experimental determinations, as mentioned in the research method, show the variations of the cumulative mean depth MDE(t) and the related erosion rate MDER(t), with the duration of exposure to cavitation and contain the values obtained through the experimental determinations, the analytical curves averaging these values, constructed with relations (2.1) and (2.2) and the values of the specific parameters. These diagrams, through the evolutions of the averaging curves, the dispersion of the experimental values, in different intervals, compared to the averaging curves, show the behavior and resistance of the surface structure to the cyclic stresses of microjets and shock waves generated by vibrating cavitation.According to the data from the, the parameter values are indicators of the resistance to the cavitation stress, and by comparison they serve to identify the material structure with the best resistance to the cyclic fatigue stresses of of shock waves and microjets developed by the implosion of bubbles generated by the mechanism of the vibrating cavity. It should be noted that, according to all the studies in this field [201-212], the dispersions of the experimental values, the evolution forms of the averaging curves and the values of the indicated parameters are an effect of the nature of the semi-finished product (cast state), of the parameters of the heat treatment regimes (treatment type , temperatures, durations), of the microstructure and mechanical properties (hardness, mechanical resistance to breaking, resilience, etc.).

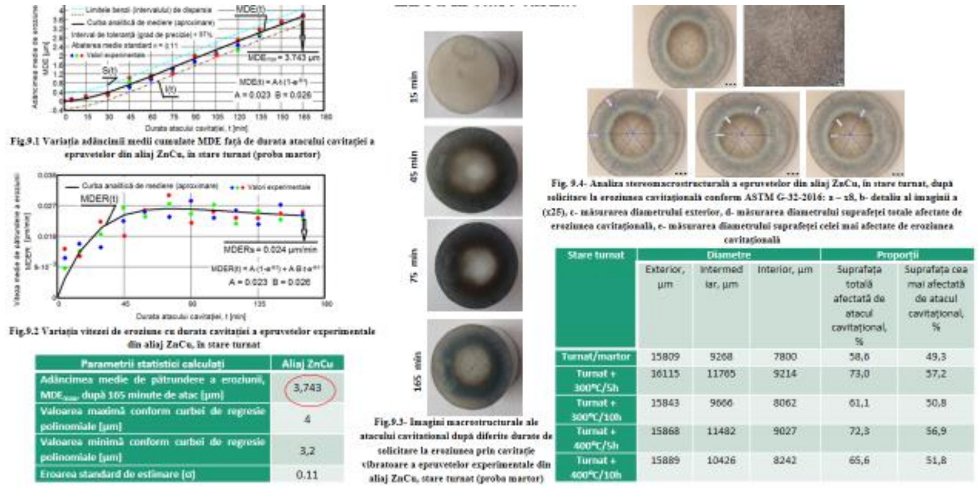

Fig.9.1 Variația adâncimii medii cumulate MDE față de durata atacului cavitației a epruvetelor din aliaj ZnCu, în stare turnat (proba martor)

Fig.9.2 Variația vitezei de eroziune cu durata cavitației a epruvetelor experimentale din aliaj ZnCu, în stare turnat

Parametrii statistici calculați	Aliaj ZnCu
Adâncimea medie de pătrundere a eroziunii, MDE_{max} după 165 minute de atac [µm]	3,743
Valoarea maximă conform curbei de regresie polinomiale [µm]	4
Valoarea minimă conform curbei de regresie polinomiale [µm]	3,2
Eroarea standard de estimare (σ)	0.11

Fig.9.3- Imagini macrostructurale ale atacului cavitațional după diferite durate de solicitare la eroziunea prin cavitație vibratoare a epruvetelor experimentale din aliaj ZnCu, stare turnat (proba martor)

Fig. 9.4- Analiza stereomacrostructurală a epruvetelor din aliaj ZnCu, în stare turnat, după solicitare la eroziunea cavitațională conform ASTM G-32-2016: a – x8, b- detaliu al imaginii a (x25), c- măsurarea diametrului exterior, d- măsurarea diametrului suprafeței totale afectate de eroziunea cavitațională, e- măsurarea diametrului suprafeței celei mai afectate de eroziunea cavitațională

Stare turnat	Diametre			Proporții	
	Exterior, µm	Intermediar, µm	Interior, µm	Suprafața totală afectată de atacul cavitațional, %	Suprafața cea mai afectată de atacul cavitațional, %
Turnat/martor	15809	9268	7800	58,6	49,3
Turnat + 300°C/5h	16115	11765	9214	73,0	57,2
Turnat + 300°C/10h	15843	9666	8062	61,1	50,8
Turnat + 400°C/5h	15868	11482	9027	72,3	56,9
Turnat + 400°C/10h	15889	10426	8242	65,6	51,8

Fig. 9.1-9.4. Cavitational erosion behavior of experimental zinc alloys from the ZnCu system in the cast state

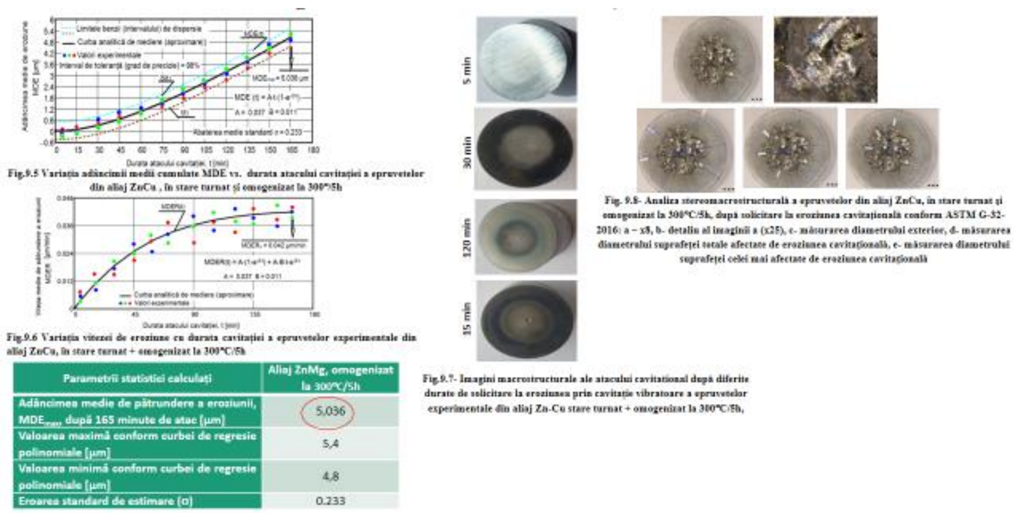

Fig.9.5 Variația adâncimii medii cumulate MDE vs. durata atacului cavitației a epruvetelor din aliaj ZnCu , în stare turnat și omogenizat la 300°/5h

Fig.9.6 Variația vitezei de eroziune cu durata cavitației a epruvetelor experimentale din aliaj ZnCu, în stare turnat + omogenizat la 300°C/5h

Parametrii statistici calculați	Aliaj ZnMg, omogenizat la 300°C/5h
Adâncimea medie de pătrundere a eroziunii, MDE_{max} după 165 minute de atac [µm]	5,036
Valoarea maximă conform curbei de regresie polinomiale [µm]	5,4
Valoarea minimă conform curbei de regresie polinomiale [µm]	4,8
Eroarea standard de estimare (σ)	0.233

Fig.9.7- Imagini macrostructurale ale atacului cavitațional după diferite durate de solicitare la eroziunea prin cavitație vibratoare a epruvetelor experimentale din aliaj Zn-Cu stare turnat + omogenizat la 300°C/5h,

Fig. 9.8- Analiza stereomacrostructurală a epruvetelor din aliaj ZnCu, în stare turnat și omogenizat la 300°C/5h, după solicitare la eroziunea cavitațională conform ASTM G-32-2016: a – x8, b- detaliu al imaginii a (x25), c- măsurarea diametrului exterior, d- măsurarea diametrului suprafeței totale afectate de eroziunea cavitațională, e- măsurarea diametrului suprafeței celei mai afectate de eroziunea cavitațională

Fig. 9.5-9.8.The cavitational erosion behavior of ZuCu alloy specimens in cast and homogenized state at 300 0C with holding time of 5 hours

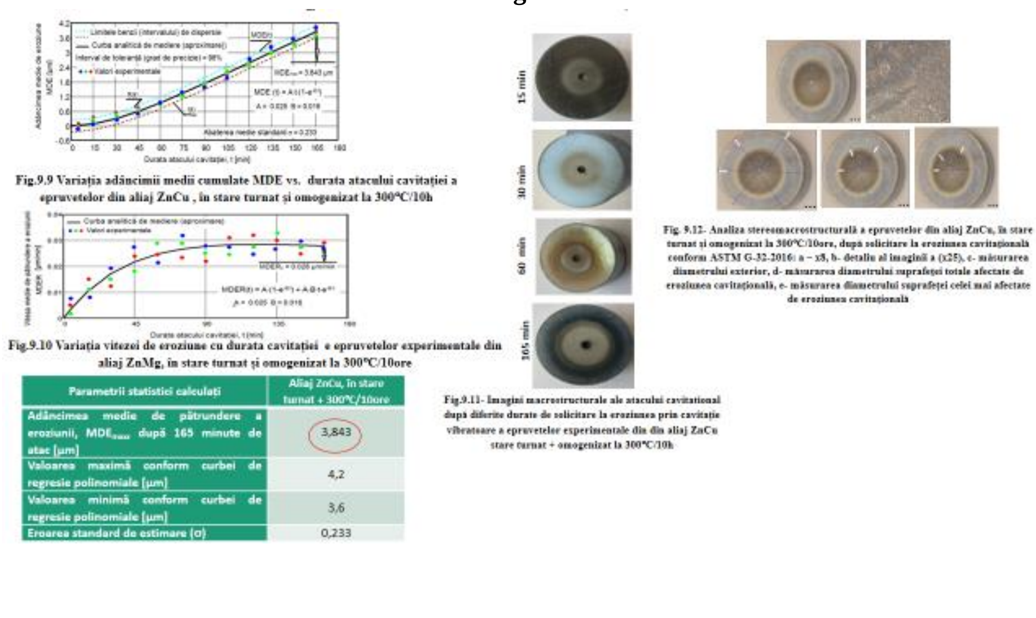

Fig.9.9 Variația adâncimii medii cumulate MDE vs. durata atacului cavitației a epruvetelor din aliaj ZnCu , în stare turnat și omogenizat la 300°C/10h

Fig.9.10 Variația vitezei de eroziune cu durata cavitației e epruvetelor experimentale din aliaj ZnMg, în stare turnat și omogenizat la 300°C/10ore

Parametrii statistici calculați	Aliaj ZnCu, în stare turnat + 300°C/10ore
Adâncimea medie de pătrundere a eroziunii, MDE_{max} după 165 minute de atac [µm]	3,843
Valoarea maximă conform curbei de regresie polinomiale [µm]	4,2
Valoarea minimă conform curbei de regresie polinomiale [µm]	3,6
Eroarea standard de estimare (σ)	0,233

Fig.9.11- Imagini macrostructurale ale atacului cavitațional după diferite durate de solicitare la eroziunea prin cavitație vibratoare a epruvetelor experimentale din din aliaj ZnCu stare turnat + omogenizat la 300°C/10h

Fig. 9.12- Analiza stereomacrostructurală a epruvetelor din aliaj ZnCu, în stare turnat și omogenizat la 300°C/10ore, după solicitare la eroziunea cavitațională conform ASTM G-32-2016: a – x8, b- detaliu al imaginii a (x25), c- măsurarea diametrului exterior, d- măsurarea diametrului suprafeței totale afectate de eroziunea cavitațională, e- măsurarea diametrului suprafeței celei mai afectate de eroziunea cavitațională

Fig. 9.9-9.12.The cavitational erosion behavior of ZuCu alloy specimens in cast and homogenized state at 300 0C with holding time of 10 hours

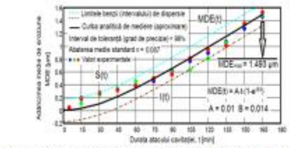

Fig.9.21 Variația adâncimii medii cumulate MDE față de durata atacului cavitației a epruvetelor din aliaj ZnCuMg, în stare turnat (proba martor)

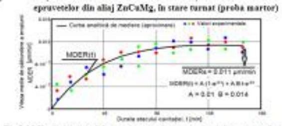

Fig.9.22 Variația vitezei de eroziune cu durata cavitației a epruvetelor experimentale din aliaj ZnCuMg, în stare turnat

Parametrii statistici calculați	Aliaj ZnCuMg
Adâncimea medie de pătrundere a eroziunii, MDE_{max} după 165 minute de atac [μm]	1,493
Valoarea maximă conform curbei de regresie polinomiale [μm]	1,6
Valoarea minimă conform curbei de regresie polinomiale [μm]	1,29
Eroarea standard de estimare (σ)	0,087

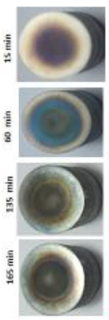

Fig.9.23- Imagini macrostructurale ale atacului cavitational după diferite durate de solicitare la eroziunea prin cavitație vibratoare a epruvetelor experimentale din aliaj ZnCuMg, stare turnat (proba martor)

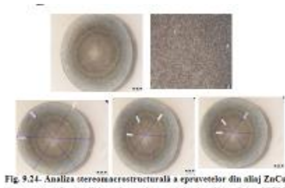

Fig. 9.24- Analiza stereomacrostructurală a epruvetelor din aliaj ZnCuMg, în stare turnat, după solicitare la eroziunea cavitațională conform ASTM G-32-2016: a – x8, b- detaliu al imaginii a (x25), c- măsurarea diametrului exterior, d- măsurarea diametrului suprafeței totale afectate de eroziunea cavitațională, e- măsurarea diametrului suprafeței celei mai afectate de eroziunea cavitațională

Stare turnat	Diametre			Proporții	
	Exterior, µm	Intermediar, µm	Interior, µm	Suprafața totală afectată de atacul cavitațional, %	Suprafața cea mai afectată de atacul cavitațional, %
Martor	14589	8768	7799	60,1	53,4
Turnat + 300°C/5h	15732	11515	9260	73,2	58,9
Turnat + 300°C/10h	15882	11567	8910	72,8	56,1
Turnat + 350°C/5h	15944	11572	8716	72,5	54,7
Turnat + 350°C/10h	15898	10694	7669	67,3	48,2

Fig.9.21-9.24.The cavitational erosion behavior of experimental specimens made of ZnCuMg alloy in the cast state, with/without homogenization thermal treatment

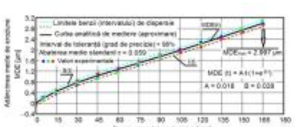

Fig.9.25 Variația adâncimii medii cumulate MDE vs. durata atacului cavitației a epruvetelor din aliaj ZnCuMg, în stare turnat și omogenizat la 300°/5h

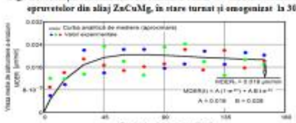

Fig.9.26- Variația vitezei de eroziune cu durata cavitației a epruvetelor experimentale din aliaj ZnCuMg, în stare turnat + omogenizat la 300°C/5h

Parametrii statistici calculați	Aliaj ZnMgCa, omogenizat la 300°C/5h
Adâncimea medie de pătrundere a eroziunii, MDE_{max}, după 165 minute de atac [μm]	2,997
Valoarea maximă conform curbei de regresie polinomiale [μm]	3,2
Valoarea minimă conform curbei de regresie polinomiale [μm]	2,8
Eroarea standard de estimare (σ)	0.059

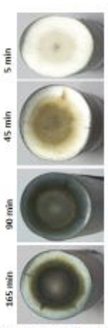

Fig.9.27- Imagini macrostructurale ale atacului cavitational după diferite durate de solicitare la eroziunea prin cavitație vibratoare a epruvetelor experimentale din aliaj ZnCuMg, stare turnat + omogenizat la 300°C/5h,

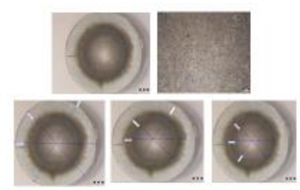

Fig. 9.28- Analiza stereomacrostructurală a epruvetelor din aliaj ZnCuMg, în stare turnat și omogenizat la 300°C/5h, după solicitare la eroziunea cavitațională conform ASTM G-32-2016: a – x8, b- detaliu al imaginii a (x25), c- măsurarea diametrului exterior, d- măsurarea diametrului suprafeței totale afectate de eroziunea cavitațională, e- măsurarea diametrului suprafeței celei mai afectate de eroziunea cavitațională

Fig. 9.25-9.28. The cavitational erosion behavior of ZnCuMg alloy specimens in cast and homogenized state at 3000C with holding time of 5 hours

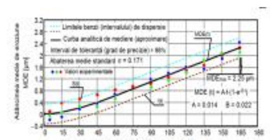

Fig.9.29 Variația adâncimii medii cumulate MDE vs. durata atacului cavitației a epruvetelor din aliaj ZnCuMg , în stare turnat și omogenizat la 300°C/10h

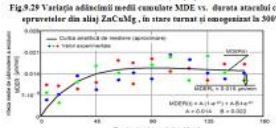

Fig.9.30 Variația vitezei de eroziune cu durata cavitației a epruvetelor experimentale din aliaj ZnCuMg, în stare turnat și omogenizat la 300°C/10ore

Parametrii statistici calculați	Aliaj ZnMg, în stare turnat + 300°C/10ore
Adâncimea medie de pătrundere a eroziunii, MDE_{max}, după 165 minute de atac [μm]	2,25
Valoarea maximă conform curbei de regresie polinomiale [μm]	2,5
Valoarea minimă conform curbei de regresie polinomiale [μm]	2,0
Eroarea standard de estimare (σ)	0,171

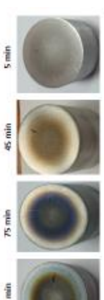

Fig.9.31- Imagini macrostructurale ale atacului cavitational după diferite durate de solicitare la eroziunea prin cavitație vibratoare a epruvetelor experimentale din aliaj ZnCuMg, stare turnat + omogenizat la 300°C/10h

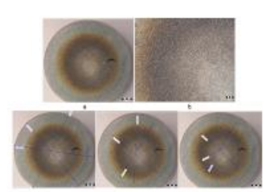

Fig. 9.32- Analiza stereomacrostructurală a epruvetelor din aliaj ZnCuMg, în stare turnat și omogenizat la 300°C/10ore, după solicitare la eroziunea cavitațională conform ASTM G-32-2016: a – x8, b- detaliu al imaginii a (x25), c- măsurarea diametrului exterior, d- măsurarea diametrului suprafeței totale afectate de eroziunea cavitațională, e- măsurarea diametrului suprafeței celei mai afectate de eroziunea cavitațională

Fig. 9.29-9.9.32. Cavitational erosion behavior of ZnCuMg alloy specimens in cast and homogenized state at 300 C with 10-hour holding time

CHAPTER 10- COMPARATIVE ANALYSIS OF THE EXPERIMENTAL RESULTS REGARDING THE CAVITATION EROSION BEHAVIOR OF SPECIMENS FROM ZnCu(Mg) SYSTEM ALLOYS

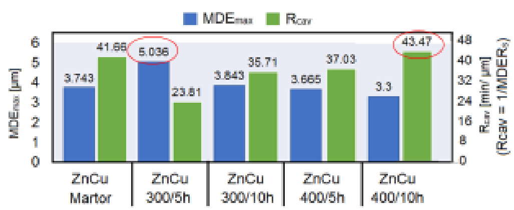

Fig. 10.5 Histograma comparării rezultatelor privind comportarea la eroziunea cavitațională a epruvetelor experimentale din aliaj ZnCu, turnat și diferite tratamente termice de omogenizare

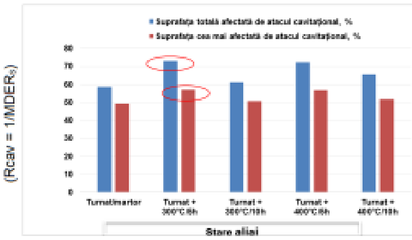

Fig. 10.6- Histograma suprafețelor afectate de cavitația probelor din aliaj ZnCu în diferite stări structurale

Fig.10.5-10.6. Quantitative comparative analysis of resistance to cavitational erosion of experimental specimens from zinc alloys of the ZnCu system

In the graph on the left side of the image we can see that: the best resistance has the samples homogenized by ZnCu at 400C/10 hours, the most cavitationally attacked is ZnCu 300/5h. In the graph on the right we can see that the surface most affected by cavitation attack it is tested ZnCu 300/5h.

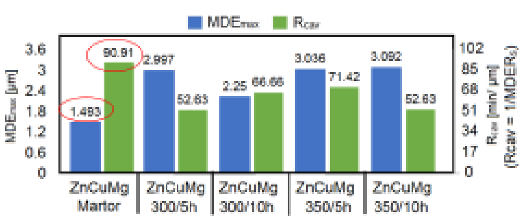

Fig. 10.7 Histograma comparării rezultatelor privind comportarea la eroziunea cavitațională a epruvetelor experimentale din aliaj ZnCuMg , turnat și diferite tratamente termice de omogenizare

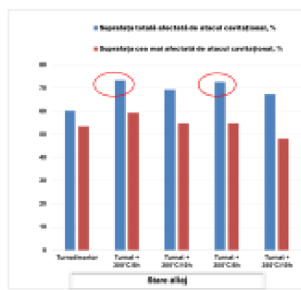

Fig. 10.8- Histograma suprafețelor afectate de cavitația probelor din aliaj ZnCuMg în diferite stări structurale

Fig.10.7-10.8. Quantitative comparative analysis of resistance to cavitational erosion of experimental specimens from zinc alloys of the ZnCuMg system

In fig. 10.7, regardless of the parameter, it shows that the best resistance has the specimens in the cast state, not thermally treated. Fig. 10.8 shows the following aspects: The surface most affected by cavitational attack, another important parameter in assessing the resistance to cavitational erosion, is about 73.2% for the sample homogenized at 300 C/5 hours, and, respectively, 72, 5% to the sample homogenized at 350 /5 hours. The sample in the cast state and homogenized at 350 C/10 hours has the smallest surface affected by cavitational erosion, respectively 48.2%. This fact shows that a structure is homogeneous, but with a large grain size confers resistance to cavitational attack compared to the inhomogeneous structure obtained after casting.

CHAPTER 11 CONCLUSIONS. ORIGINAL CONTRIBUTIONS.
PERSPECTIVES OF FUTURE RESEARCH

The work, by completing it, can bring the following contributions of own experimental research:
- The creation of new zinc alloys with superior biodegradation properties from the Zn-Cu binary system and the ZnCuMg ternary system, other than those investigated so far in the specialized literature, with well-defined chemical compositions;
- The complete physico-mechanical and structural characterization of the new biodegradable zinc alloys and the realization of a structural correlation of the influence of the alloying elements on the behavior of these alloys either cavitationally or biodegradable;
-Investigation of the cavitational erosion behavior of the new experimental zinc alloys in the ZnCu and ZnCuMg system through a complete study, correlated with the different structural states of the alloys;
- Investigating the biodegradation behavior of the new zinc alloys by performing laboratory tests in human simulant fluid (SBF) at different immersion times, respectively 3,7,14,21,28 and 35 days and presenting the comparative values obtained by performing the curves of variation: degradation rate and pH as a function of immersion time.
-The comparison of the experimental results from this paper with the data from the specialized literature shows that alloying changes the biodegradation behavior of zinc-based alloys, on the one hand, and the values obtained are comparative and even unexpected for a complex alloy chosen in the paper.
- Fractographic analysis of cavitationally eroded surfaces, highlighting the mechanism of the phenomenon and the compositional change through alloying of these alloys;
- Original assessment of cavitationally eroded surfaces through quantitative stereomacrostructural analyses, highlighting the extension of both the total cavitationally attacked surface and the most cavitationally attacked surface. Thus, the total surfaces affected by cavitational erosion in cast alloys are around 60%, while in homogenized alloys it increases up to 70%. Also, the surfaces most affected by cavitational attack are smaller in cast alloys, about 55-50%, compared to homogenized alloys, up to 60%.

B**IBLIOGRAFIE**

[214]Antoniac, I.; Miculescu, M.; Mănescu, V.; Stere, A.; Quan, P.H.; Păltânea, G.; Robu, A.; Earar,K.

[215] Magnesium-Based Alloys Used in Orthopedic Surgery. *Materials* **2022**, *15*, 1148.

[216] Antoniac, I.V.; Filipescu, M.; Barbaro, K.; Bonciu, A.; Birjega, R.; Cotrut, C.M.; Galvano, E.; Fosca, M.; Fadeeva, I.V.; Vadalà, G.; et al.

[217] Iron Ion-Doped Tricalcium Phosphate Coatings Improve the Properties of Biodegradable Magnesium Alloys for Biomedical Implant Application. *Adv. Mater. Interfaces* **2020**, *7*, 2000531

[218] I Antoniac, V Manescu, A Antoniac, G Paltanea

[219] Magnesium-based alloys with adapted interfaces for bone implants and tissue engineering

[220] Regenerative Biomaterials 10, rbad095,140

[221] I Antoniac, V Manescu, G Paltanea, A Antoniac, IV Nemoianu, MI Petrescu, ...

[222] Additive manufactured magnesium-based scaffolds for tissue engineering

[223] Materials 15 (23), 8693

[224] B Yuan, H Chen, R Zhao, X Deng, G Chen, X Yang, Z Xiao, A Aurora, ...

[225] Construction of a magnesium hydroxide/graphene oxide/hydroxyapatite composite coating on Mg–Ca–Zn–Ag alloy to inhibit bacterial infection and promote bone regeneration

[226] Bioactive materials 18, 354-367 62, 2022

[227] H Chen, B Yuan, R Zhao, X Yang, Z Xiao, A Aurora, BA Iulia, X Zhu, ...

[228] Evaluation on the corrosion resistance, antibacterial property and osteogenic activity of biodegradable Mg-Ca and Mg-Ca-Zn-Ag alloys

[229] Journal of Magnesium and Alloys 10 (12), 3380-3396

[230] Rau, J.V.; Antoniac, I.; Filipescu, M.; Cotrut, C.; Fosca, M.; Nistor, L.C.; Birjega, R.; Dinescu, M. Hydroxyapatite Coatings on Mg-Ca Alloy Prepared by Pulsed Laser Deposition: Properties and Corrosion Resistance in Simulated Body Fluid. *Ceram. Int.* **2018**, *44*, 16678–16687.

[231] Antoniac, I.; Miculescu, F.; Cotrut, C.; Ficai, A.; Rau, J.V.; Grosu, E.; Antoniac, A.; Tecu, C.; Cristescu, I. Controlling the Degradation Rate of Biodegradable Mg–Zn-Mn Alloys for Orthopedic Applications by Electrophoretic Deposition of Hydroxyapatite Coating. *Materials* **2020**, *13*, 263.

[232] R Adam, I Antoniac, S Negoiță, C Moldovan, E Rusu, C Orban, ...

[233] In Vivo Study of Local and Systemic Responses to Clinical Use of Mg–1Ca Bioresorbable Orthopedic Implants

[234] Diagnostics 12 (8), 1966

[235] Quan, P.H.; Antoniac, I.; Miculescu, F.; Antoniac, A.; Manescu, V.; Robu, A.; Bița, A.I.; Miculescu, M.; Saceleanu, A.; Bodog, A.D.; et al. Fluoride Treatment and In Vitro Corrosion Behavior of Mg-Nd-Y-Zn-Zr Alloys Type. *Materials* **2022**, *15*, 566.

[236] Streza, A.; Antoniac, A.; Manescu, V.; Paltanea, G.; Robu, A.; Dura, H.; Verestiuc, L.; Stanica, E.; Voicu, S.I.; Antoniac, I.; et al. Effect of Filler Types on Cellulose-Acetate-Based Composite Used as Coatings for Biodegradable Magnesium Implants for Trauma. *Materials* **2023**, *16*, 554.

[237] Bița, A.-I.; Antoniac, I.; Miculescu, M.; Stan, G.E.; Leonat, L.; Antoniac, A.; Constantin, B.; Forna, N. Electrochemical and In Vitro Biological Evaluation of Bio-Active Coatings Deposited by Magnetron Sputtering onto Biocompatible Mg-0.8Ca Alloy. *Materials* **2022**, *15*, 3100.

[238] Bone Regeneration Induced by Patient-Adapted Mg Alloy-Based Scaffolds for Bone Defects: Present and Future Perspectives

LISTA LUCRARILOR PUBLICATE

Articole ISI web of knowledge

1. Gheorghe Cristina Maria, **Petre Gabriela**; Trante, Octavian; Milea Claudia Georgiana; Ghiban, Brandusa -CORROSION BEHAVIOUR OF ZAMAK COMPONENTS IN A HEARING AID, UNIVERSITY POLITEHNICA OF BUCHAREST SCIENTIFIC BULLETIN SERIES B-CHEMISTRY AND MATERIALS SCIENCE, Volume 83, Issue 4, Page, 251-262
2. **GABRIELA CIUNGU**, LAVINIA MADALINA MICU, ILARE BORDEASU, CRISTINA MARIA IORDACHE, BRANDUSA GHIBAN, CRISTIAN GHERA- RESEARCH OF THE CAVITATION RESISTANCE OF A BIODEGRADABLE ALLOY Zn-Cu, U.P.B. Sci. Bull., Series …, Vol. …, Iss. …, 201 ISSN 1223-7027 (in curs de publicare)

Articole cotate BDI

1. Iordache (Gheorghe) Cristina Maria, Nicolae Alexandru Luca, Bordeasu Ilare, **Ciungu Gabriela**, Ghiban Brandusa – Cavitational Erosion Behavior of a Biodegradable Alloy from the Zn-Mg System for Biomedical Applications, Tribology in Industry, DOI: 10.24874/ti.1548.09.23.11, 2024, 46(2), pp. 315–323
2. Luca Nicolae Alexandru, Bordeasu Iordache, **Ciungu(Petre) Gabriela**, Iordache (Gheorghe) Cristina Maria, Miculescu Marian, Madalina Micu- Heat Treatment Influence on the Cavitational Erosion Zn-Mg Behavior Used for Biomedical Applications, Tribology in Industry, DOI: 10.24874/ti.1604.11.23.01, 2024, 46(2), pp. 270–282

Lucrări prezentate în cadrul unor conferințe naționale/ participare internatională

1. Brândușa Ghiban, Iulian Vasile Antoniac, Cristina Maria Iordache, **Gabriela Petre**, Aurora Antoniac New biodegradable zinc alloys for biomedical applications , BIOMAH 2024 (Roma)
2. Iordache (Gheorghe) Cristina Maria, Nicolae Alexandru Luca, Bordeasu Ilare, **Ciungu(Petre) Gabriela,** Ghiban Brandusa - Cavitational Erosion Behavior of a Biodegradable Alloy from the Zn-Mg System for Biomedical Applications- on-line presentation, SERBIATRIB'23, 18th International Conference on Tribology
3. Luca Nicolae Alexandru, Bordeasu Iordache, **Ciungu(Petre) Gabriela**, Iordache (Gheorghe) Cristina Maria, Miculescu Marian, Madalina Micu- Heat Treatment Influence on the Cavitational Erosion Zn-Mg Behavior Used for Biomedical Applications, on-line presentation SERBIATRIB'23, 18th International Conference on Tribology
4. C.M. Iordache (Gheorghe), **G.Ciungu(Petre),** B.Ghiban- Structural modifications in ZnMg(Ca) alloys for orthopedic applications , ROMAT 2022
5. **G. Ciungu (Petre**), C.M. Iordache (Gheorghe), B. Ghiban - Structural modifications in ZnCu(Mg) alloys for cardiovascular applications, ROMAT 2022
6. **Gabriela Ciungu**, Cristina Maria Iordache, Robert Ciocoiu, Brandusa Ghiban-Structural characterization of a new ZnCu(Mg) biodegradable alloy, BioReMed 2023
7. Cristina Maria Iordache**, Gabriela Ciungu**, Marian Minculescu, Robert Ciocoiu, Brandusa Ghiban-Heat Treatment Influence on The Mechanical and Structure properties of a new ZnMg(Ca) biodegradable alloy, BioReMed 2023